SUPPORTING INFORMATION

Machine Intelligence Accelerated Design of Conductive MXene Aerogels with Programmable Properties

Snehi Shrestha[a], Kieran James Barvenik[b], Tianle Chen[a], Haochen Yang[a], Yang Li[a], Meera Muthachi Kesavan[a], Joshua M. Little[a], Eleonora Tubaldi[b,c,*], Po-Yen Chen[a,c,*]

[a] Department of Chemical and Biomolecular Engineering, University of Maryland, College Park, MD 20742, United States

[b] Department of Mechanical Engineering, University of Maryland, College Park, MD 20742, United States

[c] Maryland Robotics Center, College Park, MD 20742, United States

* Email: etubaldi@umd.edu (E.T.)

checp@umd.edu (P.-Y. C.)

Keywords: Machine learning; collaborative robots; $Ti_3C_2T_x$ MXene nanosheets; conductive aerogels; finite element simulations; wearable thermal management.

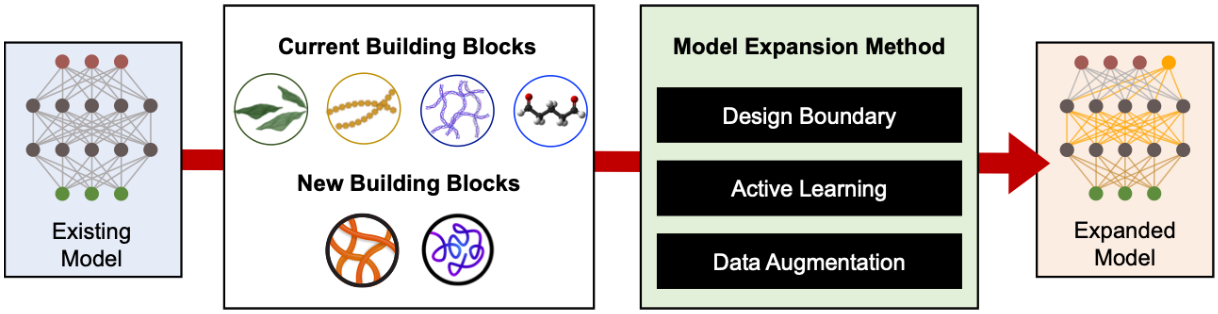

Fig. S1. Schematic illustration of a model expansion strategy.

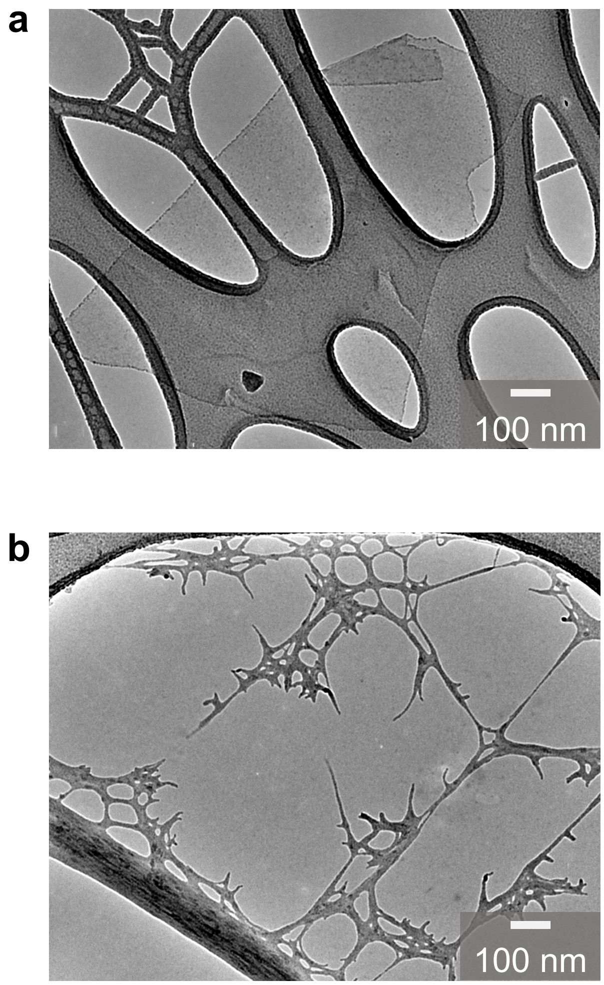

Fig. S2. TEM images of MXene nanosheets and CNFs. (**a**) TEM image of MXene nanosheets. (**b**) TEM image of CNFs.

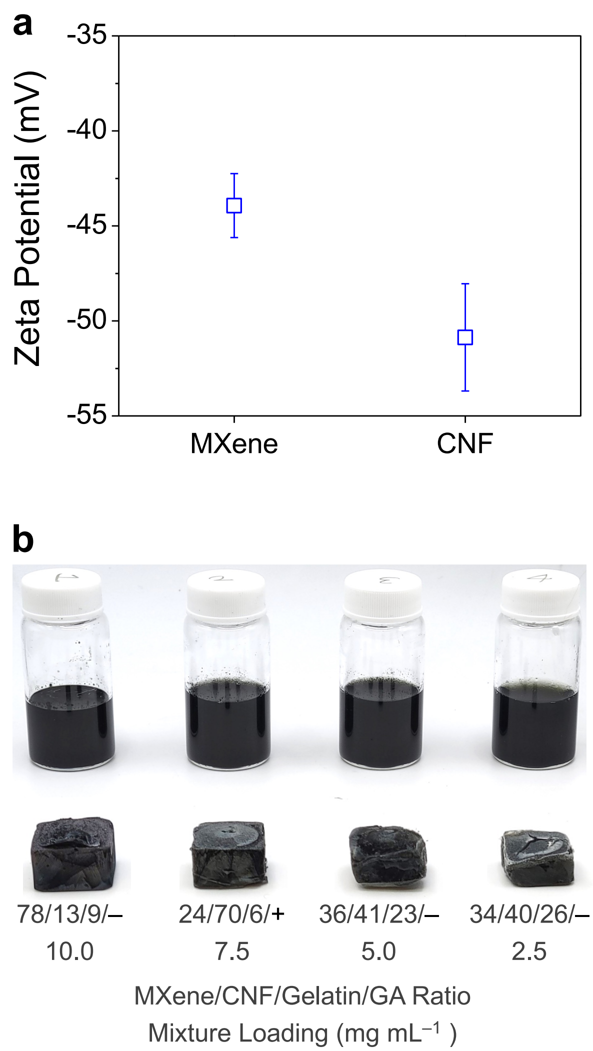

Fig. S3. Fabrication of conductive aerogels with tunable compositions and mixture loadings. (**a**) Zeta potentials of MXene and CNF dispersions. (**b**) Photo of various MXene/CNF/gelatin/GA mixtures with various ratios and mixture loadings as well as the resulting conductive aerogels.

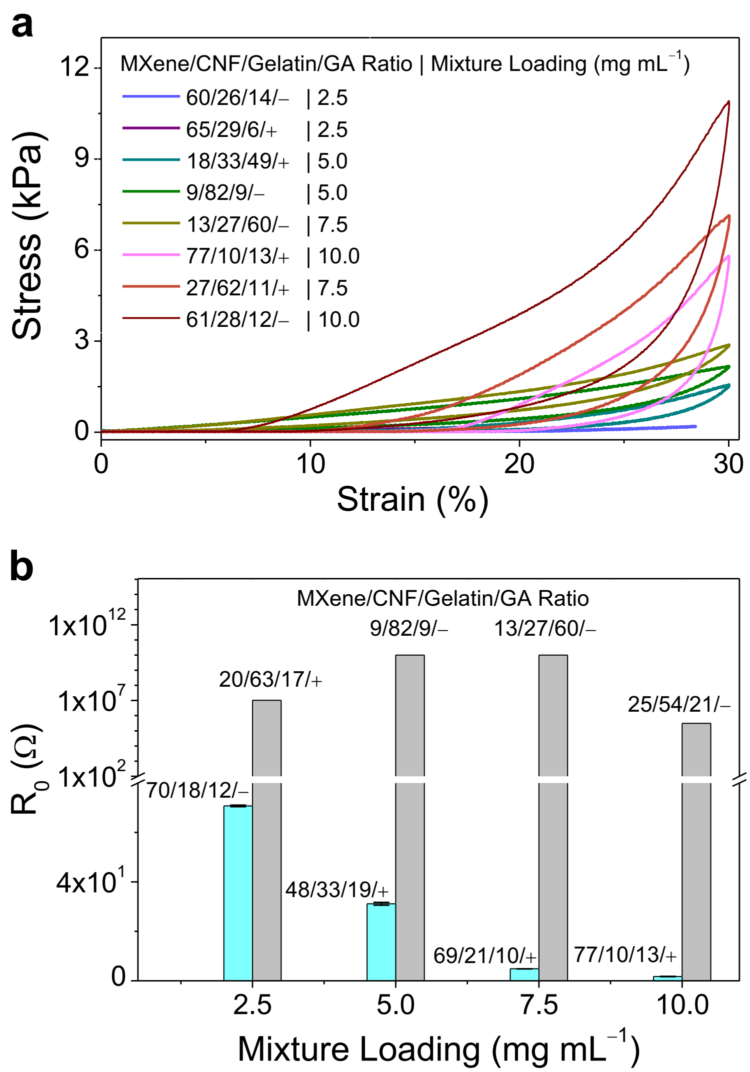

Fig. S4. Tunable mechanical and electrical properties of conductive aerogels. The mechanical and electrical properties of conductive aerogels, such as σ_{30} and R_0, showed complex and nonlinear correlations with the MXene/CNF/gelatin/GA ratios and the solid contents of aqueous mixtures (abbreviated as mixture loadings). (**a**) Stress–strain curves of eight conductive aerogels with different MXene/CNF/gelatin/GA ratios and mixture loadings. (**b**) R_0 values of eight conductive MXene aerogels with different MXene/CNF/gelatin/GA ratios and mixture loadings.

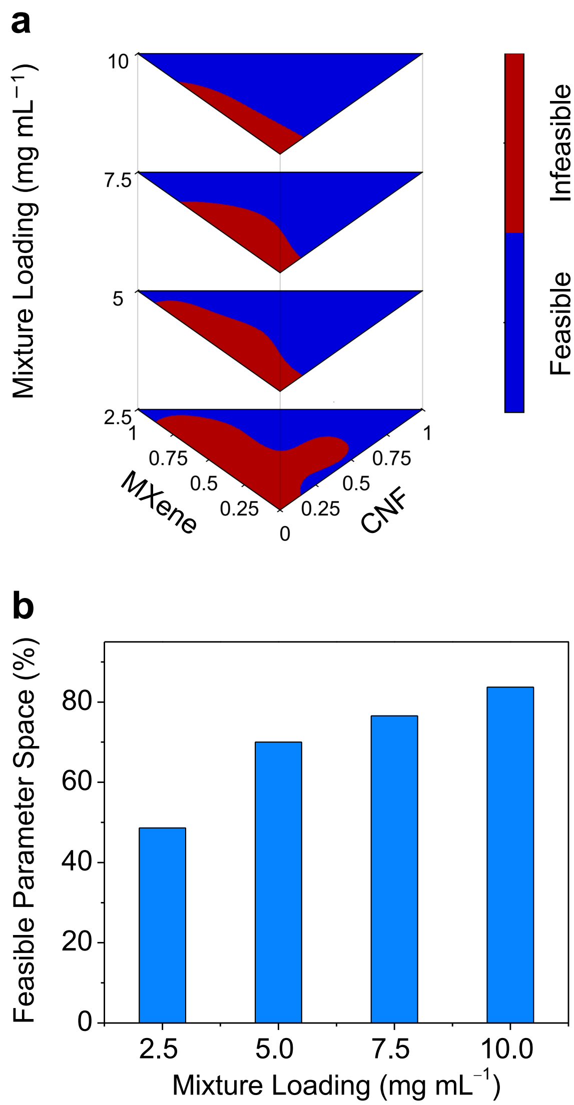

Fig. S5. Feasible parameter space of conductive aerogels. (**a**) Binary maps representing the feasible parameter space of obtaining *A*-grade conductive aerogels. (**b**) As the mixture loading decreased from 10.0 to 2.5 mg mL^{-1}, the area of the feasible parameter space decreased from 83.7% to 48.6%, respectively.

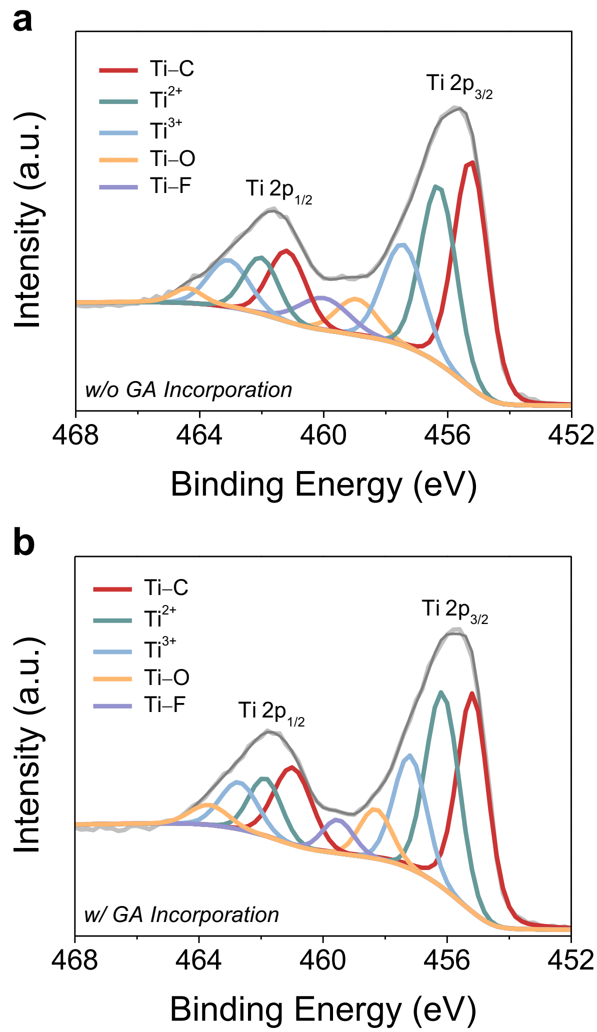

Fig. S6. Ti 2p spectra of MXene/CNF aerogels without and with GA incorporation. (**a**) Ti 2p spectrum of the conductive aerogel without GA incorporation (at the MXene/CNF/gelatin/GA ratio of 80/20/0/– and the mixture loading of 10 mg mL^{-1}). (**b**) Ti 2p spectrum of the conductive aerogel with GA incorporation (at the MXene/CNF/gelatin/GA ratio of 80/20/0/+ and the mixture loading of 10 mg mL^{-1}).

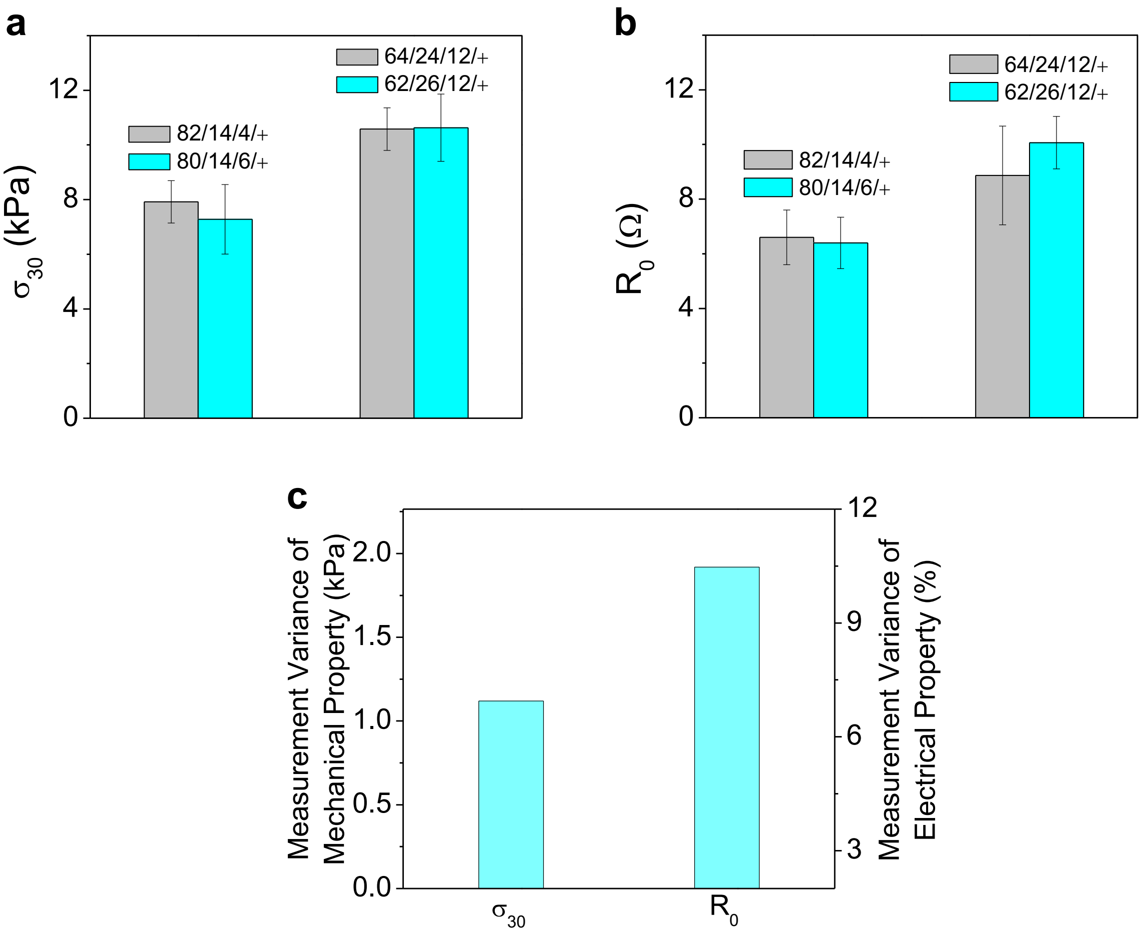

Fig. S7. Empirical evidence for implementing the UIP Method. With slight variations of MXene/CNF/gelatin/GA ratios, the resulting conductive aerogels demonstrated similar (**a**) σ_{30} and (**b**) R_0 values. The above conductive aerogels demonstrated the same mixture loading of 10 mg mL^{-1}. (**c**) By characterizing 3–4 replicates of conductive aerogels, measurement variations were observed in the σ_{30} (~1.1 kPa) and R_0 (~10.1%) values.

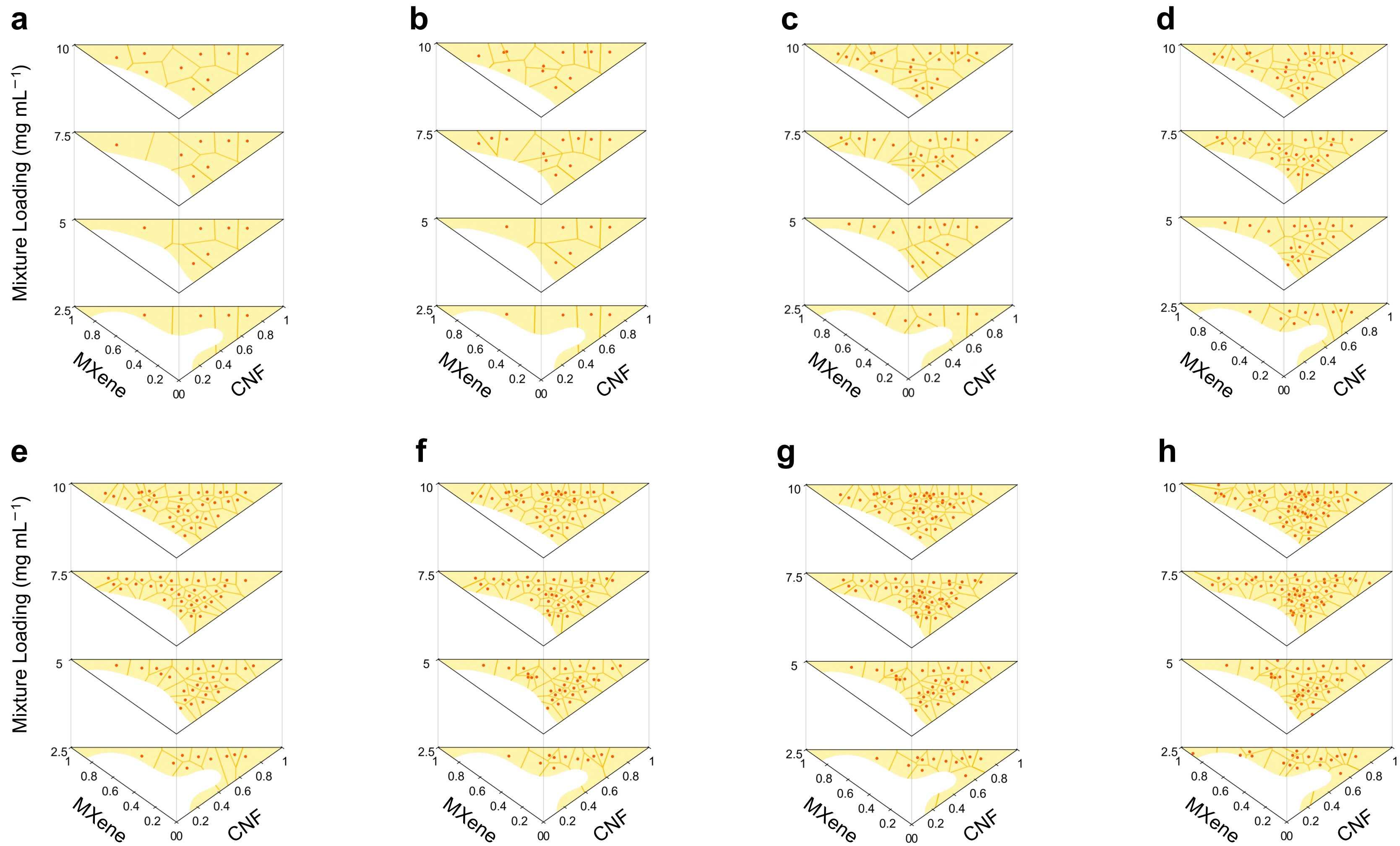

Fig. S8. 2D Voronoi tessellation diagrams from loop #1 to loop #8.

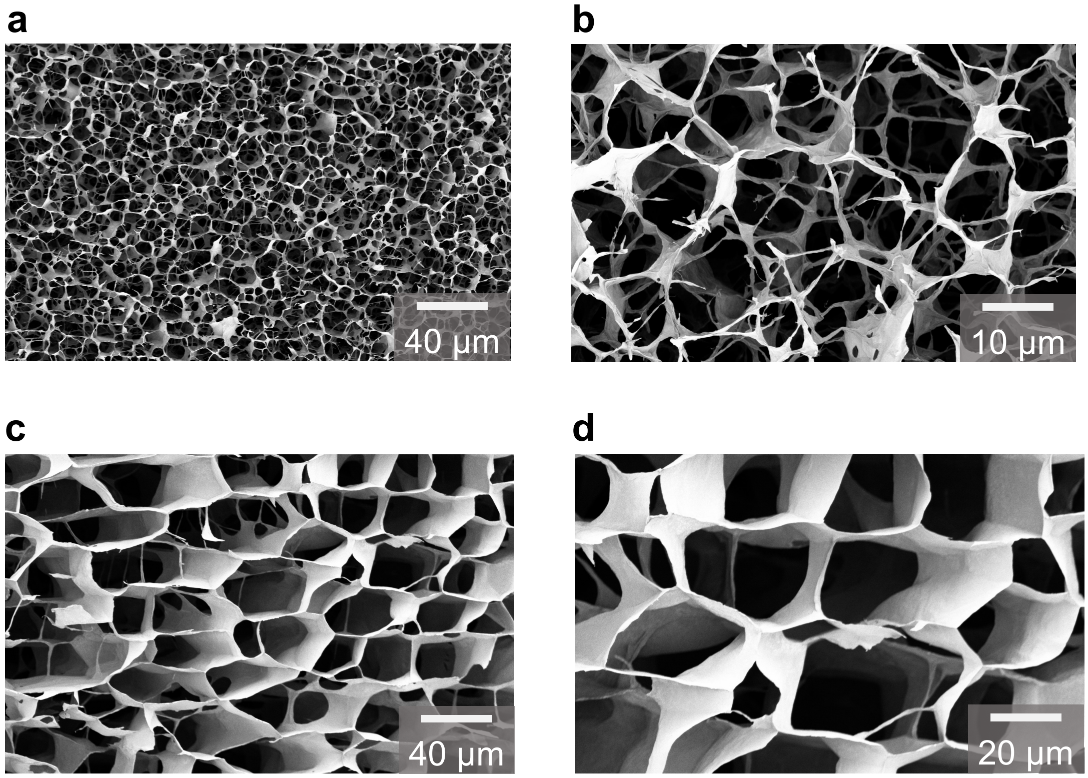

Fig. S9. SEM images of model-suggested conductive aerogels. (**a**)(**b**) SEM images of a model-suggested conductive aerogel that met the design request #1. The design request #1 was σ_{30} >10 kPa, and the champion model suggested recipe #9 (MXene/CNF/gelatin/GA ratio of 22/66/12/+ and mixture loading of 10.0 mg mL^{-1}). (**c**)(**d**) SEM images of a model-suggested conductive aerogel that met the design request #2. The design request #2 was σ_{30} >10 kPa and R_0 <10 Ω, and the champion model suggested recipe #14 (MXene/CNF/gelatin/GA ratio of 72/22/6/+ and mixture loading of 10.0 mg mL^{-1}).

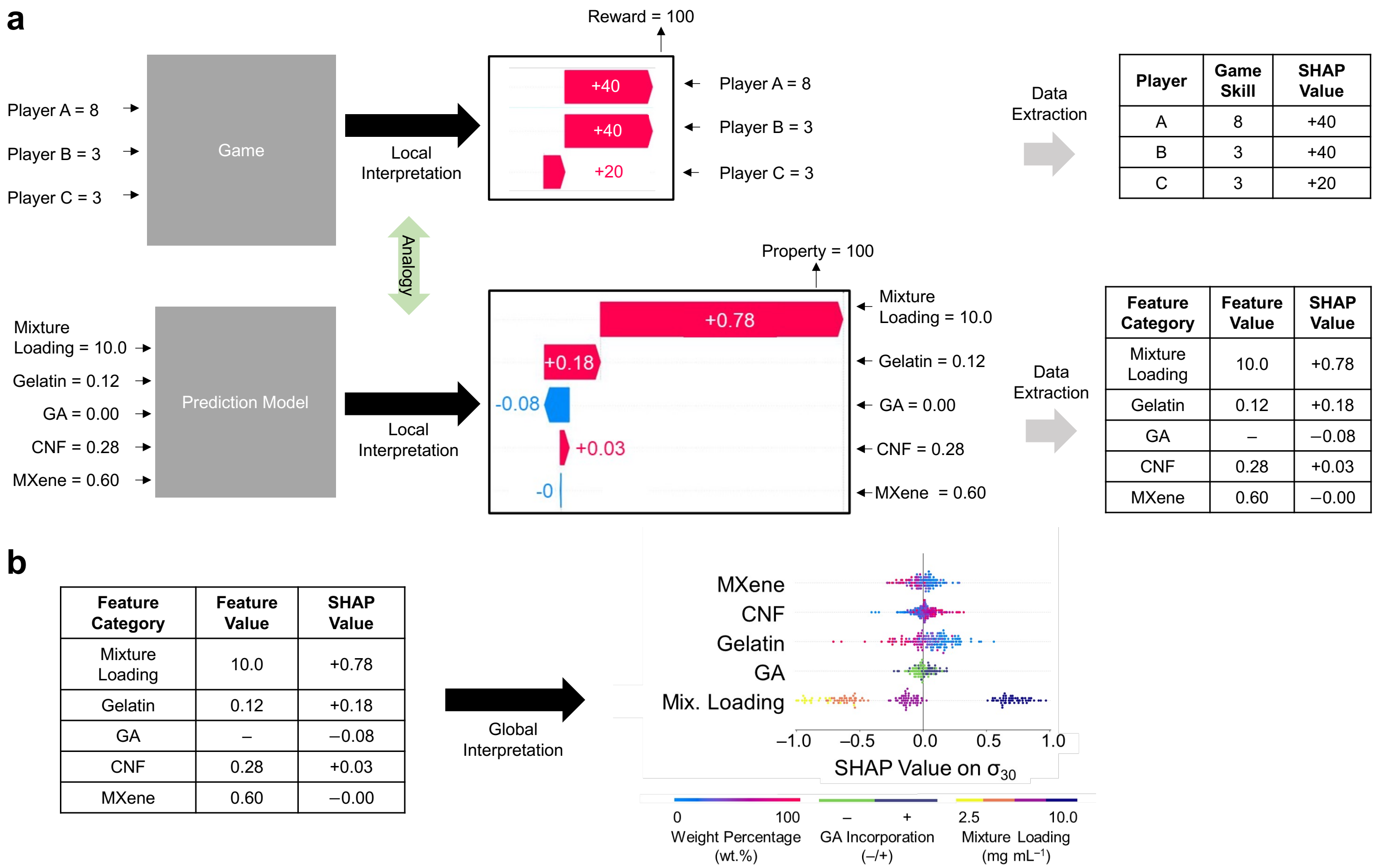

Fig. S10. Working mechanism of SHAP. (**a**) An analogy between the interpretation of a specific game and the interpretation of a prediction model. The red and blue bars represent the positive and negative SHAP values, respectively. (**b**) Figure plotting to get the global interpretation of the prediction model by using the SHAP values of every feature for every data point.

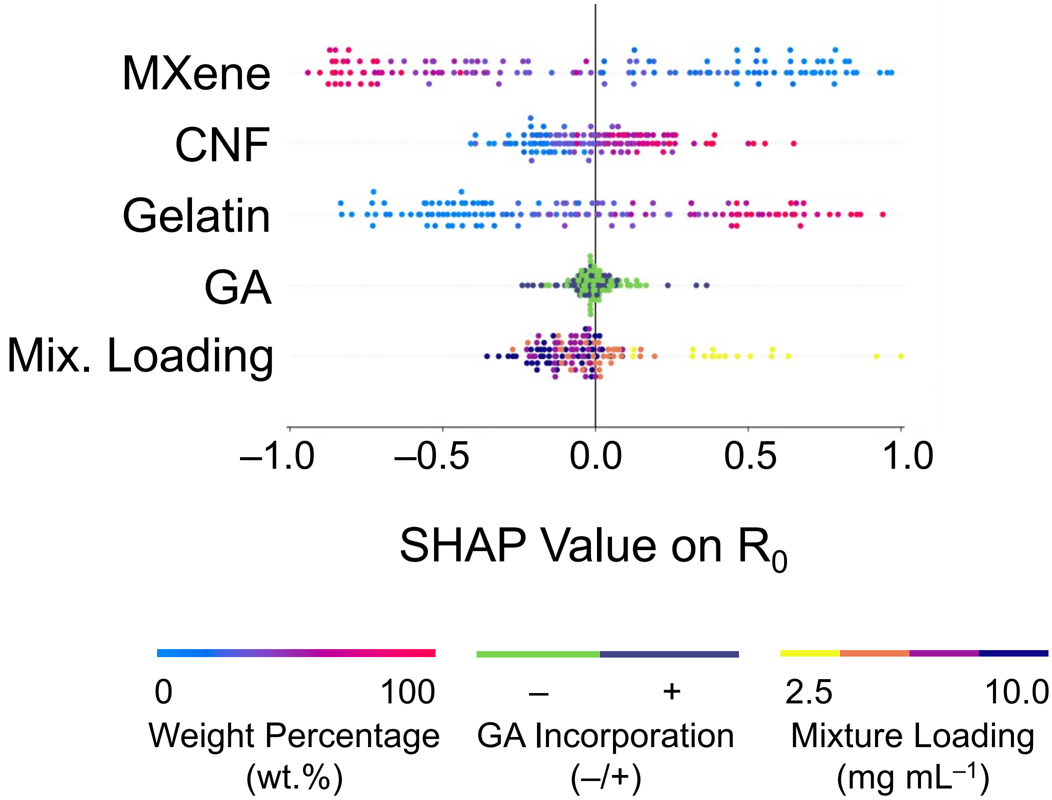

Fig. S11. SHAP values of MXene, CNF, gelatin, and GA loadings and the mixture loadings on R_0**.**

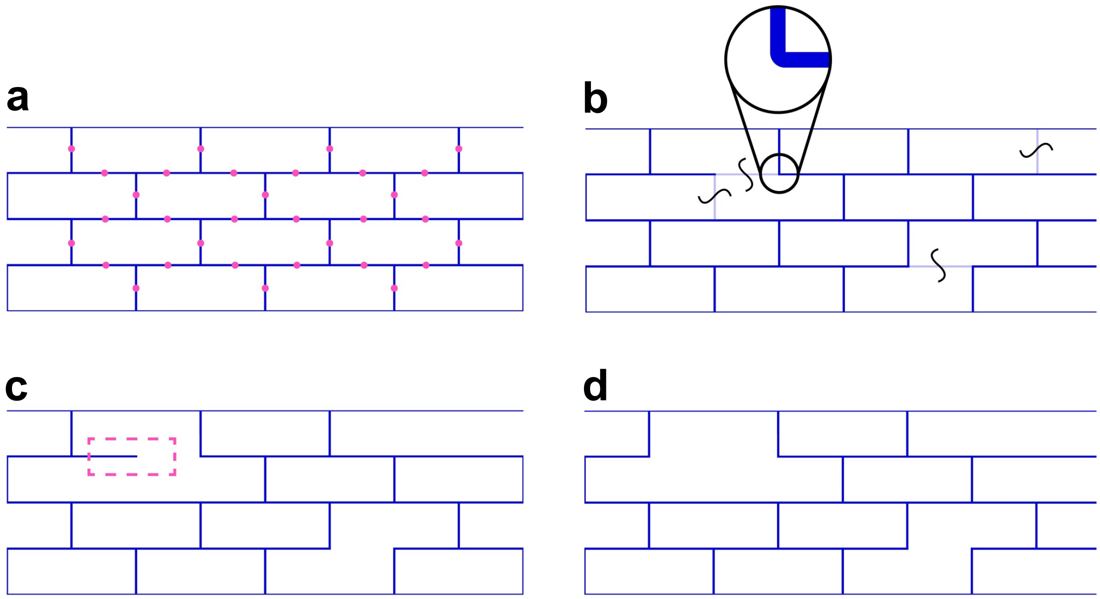

Fig. S12. Numerical geometries for FE models. (**a**) Every wall segment within the lattice that could accommodate a valid discontinuity was cataloged into an array. (**b**) A random assortment of locations was selected to host wall discontinuities. At the designated locations, the wall segments were completely eliminated, leaving rounded corners at the adjoining wall intersections to facilitate contacts. (**c**) Independent wall sections that did not bear load and could potentially cause problems for simulated contact were removed. (**d**) The final geometry with random wall discontinuities was generated.

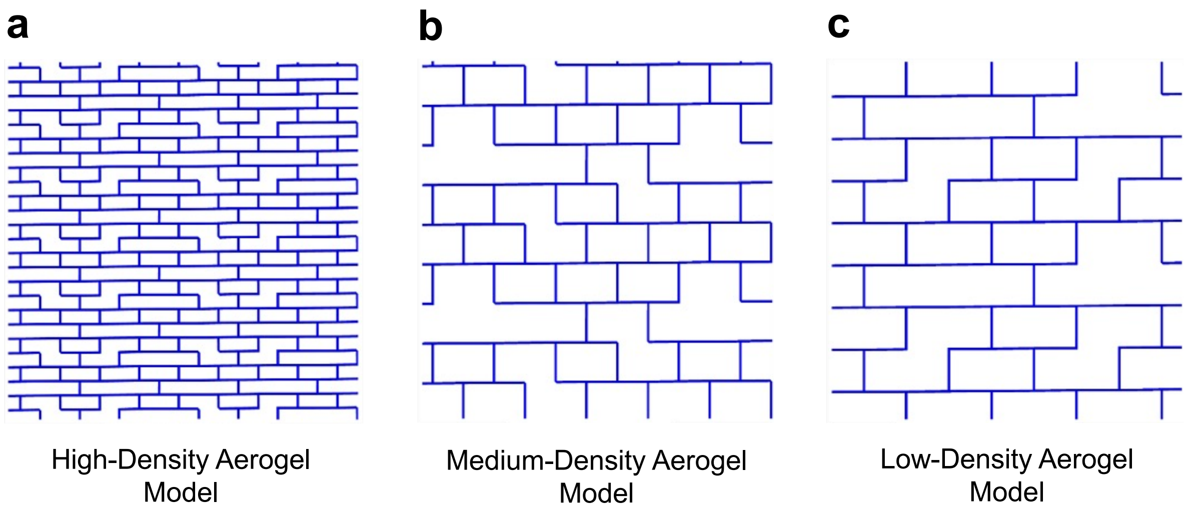

Fig. S13. High-, medium-, low-density aerogel models at their relaxed states. (**a**) High-density aerogel model. (**b**) Medium-density aerogel model. (**c**) Low-density aerogel model.

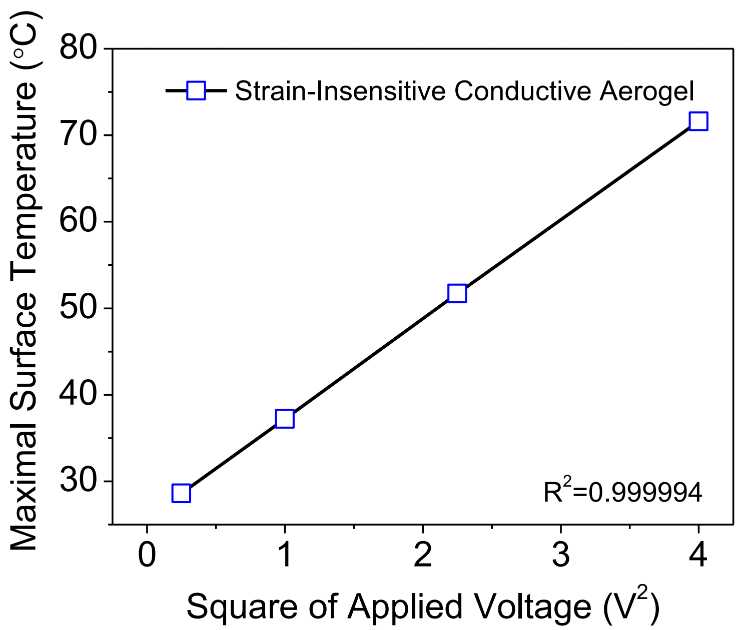

Fig. S14. Joule's law of strain-insensitive conductive aerogels. Maximal surface temperature of a strain-insensitive conductive aerogel (at the MXene/CNF/gelatin/GA ratio of 78/13/9/– and the mixture loading of 7.5 mg mL^{-1}) were linearly correlated with the square of applied voltages.

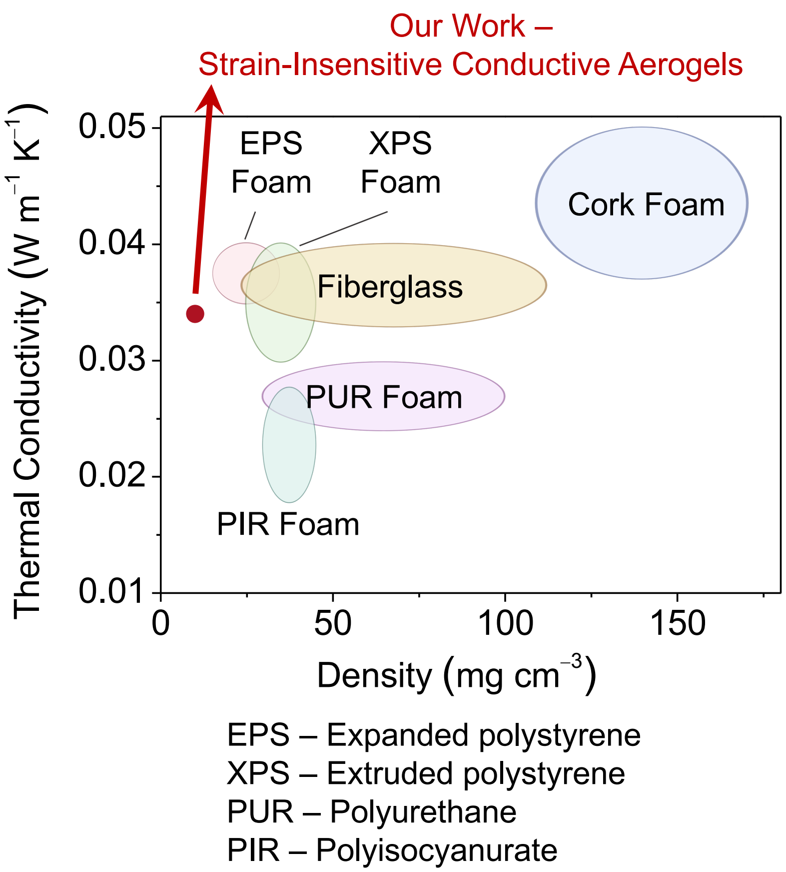

Fig. S15. Comparison of strain-insensitive conductive aerogels with commercial foam materials in terms of thermal conductivity and density. The data of commercial foam materials are collected from the literature.[1]

Note S1. Rationale of building block selection and model expansion strategy.

The rationale behind selecting $Ti_3C_2T_x$ MXene nanosheets, CNFs, and gelatin for the fabrication of conductive aerogels results from the synergistic effects of these building blocks on the aerogel's properties.

1. <u>$Ti_3C_2T_x$ MXene nanosheets:</u>

- Electrical conductivity: $Ti_3C_2T_x$ MXene nanosheets, belonging to a class of two-dimensional materials, are known for their high electrical conductivity, which makes them a preferred choice for boosting the electrical conductivity of conductive aerogels.
- Surface chemistry: With abundant functional groups like –OH, –F, and –O on the MXene surfaces, MXene nanosheets can form stable interactions with other building blocks (such as CNFs and gelatin) and enhance the structural stability of the resulting aerogels.

2. <u>CNFs:</u>

- Structural reinforcement: CNFs are renowned for their superior mechanical strength and stiffness, acting as reinforcement units in the conductive aerogels.
- High aspect ratio: The high aspect ratio of CNFs can facilitate the formation of a percolated network throughout the conductive aerogel, leading to enhanced mechanical resilience.
- Hydrophilicity: The inherent hydrophilicity of CNFs aids in the uniform distribution of other building blocks within the aerogel structure.

3. <u>Gelatin:</u>

- Gelling agent: Gelatin, a natural biopolymer, excels as a gelling agent, especially when combined with crosslinking agents, such as glutaraldehyde.

- Affinity to other building blocks: Because of its ability to form robust molecular interactions, gelatin can bridge MXenes and CNFs effectively, creating potential hybrid systems of conductive aerogels.

The choice of building blocks is crucial in determining the achievable functions of conductive aerogels. To include a fifth building block, a model expansion method is recommended. As shown in **Fig. S1**, additional active learning loops should be performed under the guidance of the prediction model. During the model expansion phase, additional experiments are required to refine the SVM classifier and to update the ANN-based model. By strategically selecting new components in tandem with the model expansion method, the prediction model can consistently enlarge its parameter space and broadened the range of achievable functions. However, model expansion demands more active loops, resulting in increased time and costs. Therefore, developing autonomous fabrication and characterization platforms can boost data collection efficiency and reduce the human workload. Also, creating an open database for the broader community could be beneficial.

Note S2. Estimated number of experiments required to build an extensive dataset for conductive aerogels.

For the composition labels, three degrees of freedom (DOFs) are identified for the fabrication of conductive aerogels. For the loading label of conductive aerogels, one DOF is identified. Considering a step size of 2.0 wt.% for the MXene, CNF, and gelatin loadings, two options (+/–) for the GA incorporation, and four mixture loadings, a total number of experiments required to construct an extensive dataset is estimated to be 5,300. In addition, two property labels, including σ_{30} and R_0, need to be collected for each conductive aerogel.

Note S3. Multi-stage AI/ML framework.

We provide in-depth justifications for the algorithmic choices in the AL/ML framework and elucidate the reasons why the selected algorithms outperform traditional or simplistic methods in terms of efficiency, accuracy, and scalability.

SVM classifier: Within the AI/ML framework, the SVM classifier acted as a crucial filtering unit for the prediction model, ensuring the model-suggested MXene/CNF/gelatin/GA ratios that produced *A*-grade conductive aerogels. In contrast to other systems rich in data, the fabrication of conductive aerogels is time-consuming and labor-intensive. In the absence of the SVM classifier, the prediction model could suggest the MXene/CNF/gelatin/GA ratios that result in lower-grade conductive aerogels, which would not be efficient for collecting high-quality data points. Therefore, a high-accuracy SVM classifier is critical to ensure the consistent production of *A*-grade conductive aerogels throughout the entire active learning loops.

ANN committee: As indicated in **Fig. 2e**, the prediction models based on alternative algorithms struggled to accurately predict the σ_{30} and R_0 values of conductive aerogels based on their MXene/CNF/gelatin/GA ratios and mixture loadings. In contrast, our prediction model, which incorporated an ANN committee, demonstrated the lowest MAE of 1.5 kPa (for σ_{30}) and MRE of 18.4% (for R_0) after the active learning loops. These results clearly show that the ANN committee is required to accurately predict the mechanical and electrical properties of conductive aerogels in a complex, non-linear system with multiple DOFs.

Data augmentation: To overcome the overfitting challenges upon the use of a small dataset, we employed a data augmentation method, specifically the UIP method, to synthesize virtual data points in the vicinity of real data points collected during the active learning loops. By feeding both real and virtual data points into the ANN committee, the prediction model demonstrated higher predictive accuracy, as evidenced by lower MRE and MAE values, as demonstrated in **Fig. 2f.**

In conclusion, the multi-stage AI/ML framework, composed of an SVM classifier, active learning loops (incorporating an ANN committee), and data augmentation, can synergistically address the data scarcity challenges encountered in the field of conductive aerogels, where the collection of high-quality data points is labor-intensive and time-consuming.

Note S4. Classification standards used for categorizing 264 samples.

Discontinuities in the aerogel's network can severely compromise its strength, structure, and functionality. The presence of cracks, deformities, and a lack of cohesion can lead to the aerogel breakage into irregular pieces or total pore structure collapse. For the SVM classifier aimed at predicting high-quality conductive aerogels, rigorous classification standards were established.

A-grade conductive aerogel standard: Monolithic, freestanding conductive aerogels with minimal imperfections and limited fragmentation are classified as *A*-grade. Aerogel samples with minor deformities, especially if localized around the edges, are also classified as *A*-grade. Conductive aerogels with fragments can also be designated as *A*-grade if they retain at least 80% of their original volume and sustain a regular structure with a uniform base and height.

B-grade conductive aerogel standard: Conductive aerogels fractured into several, yet substantial fragments, fall under *B*-grade. Although these fragments are often monolithic, freestanding, and porous, their varied shapes and sizes make them less reliable for precise mechanical and resistance measurements.

C-grade conductive aerogel standard: Highly deformed or collapsed conductive aerogel samples are categorized as *C*-grade. These samples present a loose structure, lacking the ability to stand freely.

Note S5. Training of a SVM classifier.

To facilitate the prediction model to suggest a set of suitable fabrication parameters for *A*-grade conductive aerogels, a high-accuracy SVM classifier was trained. The model training was achieved through a two-step process, including (*1*) selecting a suitable kernel function and (*2*) optimizing SVM hyperparameters. Given that the collected grades exhibited non-linear properties, we opted to use a kernel function that mapped discrete data points into a higher dimensional feature space, thereby facilitating the identification of optimal hyperplanes with maximal margin distances. We selected the Radial Basis Function (RBF) as our kernel function to handle the non-linear data points. Subsequently, we implemented Bayesian optimization with a 4-fold cross validation process to fine-tune the hyperparameter values. The SVM classifier was trained using 264 grades, which achieved a prediction accuracy of 95% based on 40 testing data points. We have recorded the Python code used for training the SVM model available on GitHub for open-source use. It can be accessed at https://github.com/oshin71/Programmable-MXene-Aerogel/blob/main/design_boundary.ipynb.

Note S6. Implementation of UIP method.

The utilization of a small dataset can potentially lead to model overfitting issues. To address this challenge, we have employed a well-known method, the UIP method, to augment the data points collected during the active learning loops. The UIP method is based on the natural principles proposed by expert users. For instance, it is observed that the property labels of a conductive aerogel remain approximately constant when there are slight variations in specific composition labels. As depicted in **Fig. S7a,b**, when the MXene/CNF/gelatin/GA ratio slightly changed from 64/24/12/+ to 62/26/12/+, the resulting conductive aerogels demonstrated similar σ_{30} and R_0 values. Moreover, we note that there are some measurement variations in the σ_{30} and R_0 values. As illustrated in **Fig. S7c**, by charactering 3–4 conductive aerogel replicates (following the same fabrication parameters), the σ_{30} and R_0 values presented the measurement variations of ~1.1 kPa and ~10.1%, respectively. In this study, the UIP method was adopted to synthesize 1,000-fold virtual data points by introducing Gaussian noises in the vicinity of 162 real data points collected during the active learning loops. We have recorded the Python code used for implementing the UIP method available on GitHub for open-source use. It can be accessed at https://github.com/oshin71/Programmable-MXene-Aerogel/blob/main/data_augmentation.ipynb.

Note S7. Calculation of *A Score* acquisition function.

A suitable acquisition function was introduced in the active learning loops to suggest the targeted data points with the highest uncertainty in the feasible design space. We defined an acquisition function as *A Score* in **Equation S1**,

$$A\ Score = L_2 \cdot \hat{\sigma} \tag{S1}$$

, where L_2 denotes the shortest mathematical distance (also called Euclidian distance) between current composition labels (within the dataset of prediction model) and targeted composition labels (not yet included in the dataset of prediction model). In particular, L_2 is calculated by **Equation S2**,

$$L_2 = \sqrt{\min_{i \in N}\left[\left(\begin{bmatrix} MXene_i \\ CNF_i \\ GEL_i \\ GA_i \\ Mixture\ Loading_i \end{bmatrix} - \begin{bmatrix} MXene_j \\ CNF_j \\ GEL_j \\ GA_j \\ Mixture\ Loading_j \end{bmatrix}\right)^2\right]} \tag{S2}$$

, where *N* is the cumulative number of data points in current dataset, $MXene_i$, CNF_i, GEL_i, GA_i, and $Mixture\ Loading_i$ represent the MXene, CNF, gelatin, GA loadings, and the mixture loading of one known data point (*i*) (already in the database), and $MXene_j$, CNF_j, GEL_j, GA_j, and $Mass\ Loading_j$ are the labels of one targeted data point (*j*) (in the feasible parameter space yet not included in the database).

On the other hand, $\hat{\sigma}$ denotes the variance of predicted property labels from the ANN committee, which is defined in **Equation S3**,

$$\hat{\sigma} = \sqrt{\frac{1}{M}\sum_{j=1}^{M}\left(\begin{bmatrix} Output_{\sigma_{30}}^{m} \\ Output_{R_0}^{m} \end{bmatrix} - \left[\begin{bmatrix} Output_{\sigma_{30}}^{Ave} \\ Output_{R_0}^{Ave} \end{bmatrix}\right]\right)^2} \tag{S3}$$

, where M is the number of ANN programs in the model committee (M = 5), $Output_{\sigma_{30}}^{m}$ and $Output_{R_0}^{m}$ are the output σ_{30} and R_0 values predicted by the m^{th} decision program, $Output_{\sigma_{30}}^{Ave}$ and $Output_{R_0}^{Ave}$ are the average σ_{30} and R_0 values predicted by the ANN committee. We have recorded the Python code used for implementing *A Score*-based active learning loops available on GitHub for open-source use. It can be accessed at the following link: https://github.com/oshin71/Programmable-MXene-Aerogel/blob/main/active_leaerning.ipynb.

Note S8. Shapley Additive exPlanations (SHAP) model interpretation method.

The SHAP analysis is a game theoretic approach to explain the output of any ML model (including the ensemble models). It can find the feature of importance inside the ML models, thus enabling the users to interpret the models. The process to find the feature importance is like finding the contribution of each player in a collaborative game.

To understand how the feature importance is found in SHAP, an example is presented below. As shown in **Fig. S10a**, there are three game players (i.e., A, B, and C). They collaborate with each other to play a game. When all of them join the game, based on their different skills in a specific game (e.g., 8, 3, and 3 for players A, B, and C.), they can achieve a 100 reward. The task is to quantify how important each player is in getting the reward. To solve this, we assume that the game players join in a specific sequence, (e.g., player A first, then player B, next player C) and the marginal rewards of each player are recorded. For example, player A is the first member with a reward of 40, then player B joins the game and brings the reward to 80, and next player C joins to bring the reward to 100. Therefore, the players' respective marginal rewards are "player A, B, C = 40, 40, 20". However, the calculated marginal reward may not accurately represent the contribution of each player. For example, when the sequence is changed from player A, B, C to player A, C, B, if players B and C have a similar skill set, the rewards are still 40, 40, and 20. Then the players' respective marginal rewards are changed to "player A, B, C = 40, 20, 40". Therefore, the sequence of how the players join the game is important.

In order to get a more accurate reward of each individual player, we need to find out the marginal reward of each player under every possible sequence. The reward for each individual player then can be the sum of these marginal rewards over the number of possible sequences (the calculation for a specific player is illustrated in **Equation S4**). For example, in the case outlined above, we can simulate the entering sequences: ABC, ACB, BCA, BAC, CAB, and CBA, and the marginal reward of each player is recorded for each sequence. Then, by averaging all of these rewards, we obtain the reward contributed from each player. This reward is the SHAP value.

$$\text{SHAP value of a player } = \frac{Sum\ of\ mariginal\ rewards\ of\ a\ specific\ player\ under\ all\ possible\ sequences}{Number\ of\ total\ possible\ sequences} \quad \textbf{(S4)}$$

Back to the feature importance analysis of the developed champion model, we can take the problem as an analogy to the above case. All composition and loading labels (i.e., MXene, CNF, gelatin, GA loadings, and mixture loading) are regarded as players, which are fed into the prediction model to obtain the property labels. The prediction process is treated as the game, and the deviation (between the predicted property label of a specific data point and the average property label from all data points) is treated as the reward. By following **Equation S5**, the SHAP value of each composition label on a specific property label can be calculated, and this value is used to measure the feature importance.

$$\text{SHAP value of a composition/loading label } = \frac{Sum\ of\ mariginal\ reward\ of\ a\ compoisiton/loading\ label\ on\ a\ specific\ property\ label\ under\ all\ possible\ sequences}{Number\ of\ total\ possible\ sequences} \quad \textbf{(S5)}$$

The above process is the interpretation of the prediction model on a specific data point which is called the local interpretation. To get the global interpretation of the prediction model over all data points, we can plot the SHAP values of every composition or loading label for every data point (**Fig. 10b**). A wider range of the SHAP value for a specific feature indicates a higher importance, and *vice versa*. We have recorded the Python code used for implementing SHAP analyses available on GitHub for open-source use. It can be accessed at https://github.com/oshin71/Programmable-

MXene-Aerogel/blob/main/plot_shaps.ipynb.

Note S9. FE model construction for conductive aerogels.

To gather a better understanding of the mechanical behaviors of conductive aerogels at different mixture loadings, we performed FE simulations with the commercially available software ABAQUS/CAE 2020. In the FE simulations, the cellular structure of a conductive aerogel was represented using a two-dimensional staggered brick-wall architecture, whose dimensions were extracted from the SEM images in **Fig. 4c**. Periodic boundary conditions were imposed to mimic the periodic nature and to mitigate the impact of boundary effects on the numerical results.[2] Based on the SEM images of conductive aerogels, analogous random discontinuities were seeded within the FE models. A 4 × 4 super cell was chosen to encapsulate a large enough bound for varying locations of seeded discontinuities, while it remained small enough to minimize computing time. The wall of conductive aerogels was modeled as an isotropic material, whose mechanical properties were acquired experimentally (see **Table S8**). In the super cell, the aerogel structure was meshed using plane strain 8-node biquadratic hybrid elements with reduced integration (ABAQUS element type CPE8RH) with second-order accuracy, and the mesh convergence has been verified. We conducted a static analysis (*STATIC step with NLGEOM=ON in ABAQUS) by linearly increasing the vertical displacement upon the compressive vertical strain of 30%, from which the σ_{30} values of conductive aerogels were derived and compared with the experimental results.

To capture the wall discontinuities of conductive aerogels, random discontinuities were seeded in the periodic structure of a FE model, based on the following method:

1. Possible discontinuity locations were created within the supercell, as shown in **Fig. S12a**.
2. A number of unit cells within the supercell were chosen to host an imperfection based on a tuning parameter (**Equation S6**),

   $$\beta_{imp} = \frac{n_i}{N_s} \quad \textbf{(S6)}$$

   , where n_i represents the number of imperfect cells within the supercell and $N_s$represents the total number of cells of the supercell. For each imperfect unit cell, a wall imperfection was seeded at a random location, and sharp corners were rounded to facilitate contacts, as shown in **Fig. S12b**.
3. Floating wall segments were removed to facilitate contact within the FE simulations, as shown in **Fig. S12c**.
4. Hard, frictionless surface-to-surface self-contacts were imposed in the aerogel structure to finalize the model construction process, as shown in **Fig. S12d**.

For all three FE models, the same β_{imp} of 0.3 was considered. Based on the first buckling mode of aerogel structures, a nodal displacement of 5% was imposed to the randomly imperfect the FE models. FE simulations were performed for three conductive aerogels at different mixture loadings (i.e., 5.0, 7.5, and 10.0 mg mL^{-1}) to construct high-, medium-, and low-density aerogel models, respectively. By exerting a vertical compressive strain of 30% on three FE models, the σ_{30} values were simulated in **Fig. 4b**, showing good agreement with the experimentally characterized σ_{30} values.

To simulate the microstructure of the conductive aerogels under compression, two different physical parameters were analyzed from the SEM images in **Fig. 4c**, including pore density (ρ) and pore aspect ratio (ψ). The ψ value was characterized by the pore shape. As depicted in **Fig. S13a–c**, the ρ of each aerogel model was quantified using **Equation S7**,

$$\rho = \frac{n_m}{N_t^p} \quad \textbf{(S7)}$$

, where n_m is the number of pixels of aerogel model and N_t^p is the total number of pixels of the 4 × 4 supercells. Similarly, the ψ of each aerogel model was calculated using **Equation S8**,

$$\psi = \frac{w}{h} \quad \textbf{(S8)}$$

, where w and h are the cell width and height, respectively (see **Table S8**). The ρ and ψ values of high-, medium-, and low-density aerogel models are presented in **Table S8**.

Table S1. Discrete grades of 264 conductive aerogels with different MXene/CNF/gelatin ratios. "*A*-grades" refer to large, intact conductive aerogels or sizable but fragmented aerogels. "*B*-grades" refer to small and fragmented aerogels. "*C*-grades" refer to extensively altered forms with inconsistent pieces.

ID (–)	MXene (wt.%)	CNF (wt.%)	Gelatin (wt.%)	Mixture Loading (mg mL^{-1})	Grade (A/B/C)
1	0	0	100	10.0	A
2	20	0	80	10.0	A
3	40	0	60	10.0	B
4	60	0	40	10.0	B
5	80	0	20	10.0	A
6	100	0	0	10.0	A
7	0	20	80	10.0	A
8	20	20	60	10.0	A
9	40	20	40	10.0	A
10	60	20	20	10.0	A
11	80	20	0	10.0	A
12	0	40	60	10.0	A
13	20	40	40	10.0	A
14	40	40	20	10.0	A
15	60	40	0	10.0	A
16	0	60	40	10.0	A
17	20	60	20	10.0	A
18	40	60	0	10.0	A
19	0	80	20	10.0	A
20	20	80	0	10.0	A
21	0	100	0	10.0	A
22	10	0	90	10.0	A
23	30	0	70	10.0	B
24	50	0	50	10.0	B
25	70	0	30	10.0	C
26	90	0	10	10.0	A
27	0	10	90	10.0	B
28	10	10	80	10.0	B
29	20	10	70	10.0	B
30	30	10	60	10.0	B
31	40	10	50	10.0	B
32	50	10	40	10.0	A

ID (–)	MXene (wt.%)	CNF (wt.%)	Gelatin (wt.%)	Mixture Loading (mg mL^{-1})	Grade (A/B/C)
33	60	10	30	10.0	A
34	70	10	20	10.0	A
35	80	10	10	10.0	A
36	90	10	0	10.0	A
37	10	20	70	10.0	A
38	30	20	50	10.0	A
39	50	20	30	10.0	A
40	70	20	10	10.0	A
41	0	30	70	10.0	A
42	10	30	60	10.0	A
43	20	30	50	10.0	A
44	30	30	40	10.0	A
45	40	30	30	10.0	A
46	50	30	20	10.0	A
47	60	30	10	10.0	A
48	70	30	0	10.0	A
49	10	40	50	10.0	A
50	30	40	30	10.0	A
51	50	40	10	10.0	A
52	0	50	50	10.0	A
53	10	50	40	10.0	A
54	20	50	30	10.0	A
55	30	50	20	10.0	A
56	40	50	10	10.0	A
57	50	50	0	10.0	A
58	10	60	30	10.0	A
59	30	60	10	10.0	A
60	0	70	30	10.0	A
61	10	70	20	10.0	A
62	20	70	10	10.0	A
63	30	70	0	10.0	A
64	10	80	10	10.0	A
65	0	90	10	10.0	A
66	10	90	0	10.0	A
67	0	0	100	7.5	A
68	10	0	90	7.5	A
69	20	0	80	7.5	B
70	30	0	70	7.5	B
71	40	0	60	7.5	C

ID (–)	MXene (wt.%)	CNF (wt.%)	Gelatin (wt.%)	Mixture Loading (mg mL^{-1})	Grade (A/B/C)
72	50	0	50	7.5	B
73	60	0	40	7.5	B
74	70	0	30	7.5	B
75	80	0	20	7.5	A
76	90	0	10	7.5	A
77	100	0	0	7.5	A
78	0	10	90	7.5	B
79	10	10	80	7.5	B
80	20	10	70	7.5	B
81	30	10	60	7.5	C
82	40	10	50	7.5	C
83	50	10	40	7.5	B
84	60	10	30	7.5	A
85	70	10	20	7.5	A
86	80	10	10	7.5	A
87	90	10	0	7.5	A
88	0	20	80	7.5	A
89	10	20	70	7.5	A
90	20	20	60	7.5	A
91	30	20	50	7.5	B
92	40	20	40	7.5	A
93	50	20	30	7.5	A
94	60	20	20	7.5	A
95	70	20	10	7.5	A
96	80	20	0	7.5	A
97	0	30	70	7.5	A
98	10	30	60	7.5	A
99	20	30	50	7.5	A
100	30	30	40	7.5	A
101	40	30	30	7.5	A
102	50	30	20	7.5	A
103	60	30	10	7.5	A
104	70	30	0	7.5	A
105	0	40	60	7.5	A
106	10	40	50	7.5	A
107	20	40	40	7.5	A
108	30	40	30	7.5	A
109	40	40	20	7.5	A
110	50	40	10	7.5	A

ID (–)	MXene (wt.%)	CNF (wt.%)	Gelatin (wt.%)	Mixture Loading (mg mL^{-1})	Grade (A/B/C)
111	60	40	0	7.5	A
112	0	50	50	7.5	A
113	10	50	40	7.5	A
114	20	50	30	7.5	A
115	30	50	20	7.5	A
116	40	50	10	7.5	A
117	50	50	0	7.5	A
118	0	60	40	7.5	A
119	10	60	30	7.5	A
120	20	60	20	7.5	A
121	30	60	10	7.5	A
122	40	60	0	7.5	A
123	0	70	30	7.5	A
124	10	70	20	7.5	A
125	20	70	10	7.5	A
126	30	70	0	7.5	A
127	0	80	20	7.5	A
128	10	80	10	7.5	A
129	20	80	0	7.5	A
130	0	90	10	7.5	A
131	10	90	0	7.5	A
132	0	100	0	7.5	A
133	0	0	100	5.0	A
134	10	0	90	5.0	B
135	20	0	80	5.0	B
136	30	0	70	5.0	B
137	40	0	60	5.0	B
138	50	0	50	5.0	C
139	60	0	40	5.0	C
140	70	0	30	5.0	B
141	80	0	20	5.0	B
142	90	0	10	5.0	A
143	100	0	0	5.0	A
144	0	10	90	5.0	B
145	10	10	80	5.0	B
146	20	10	70	5.0	B
147	30	10	60	5.0	B
148	40	10	50	5.0	C
149	50	10	40	5.0	B

ID (–)	MXene (wt.%)	CNF (wt.%)	Gelatin (wt.%)	Mixture Loading (mg mL^{-1})	Grade (A/B/C)
150	60	10	30	5.0	B
151	70	10	20	5.0	B
152	80	10	10	5.0	A
153	90	10	0	5.0	A
154	0	20	80	5.0	A
155	10	20	70	5.0	A
156	20	20	60	5.0	A
157	30	20	50	5.0	B
158	40	20	40	5.0	B
159	50	20	30	5.0	A
160	60	20	20	5.0	A
161	70	20	10	5.0	A
162	80	20	0	5.0	A
163	0	30	70	5.0	A
164	10	30	60	5.0	A
165	20	30	50	5.0	A
166	30	30	40	5.0	A
167	40	30	30	5.0	A
168	50	30	20	5.0	A
169	60	30	10	5.0	A
170	70	30	0	5.0	A
171	0	40	60	5.0	A
172	10	40	50	5.0	A
173	20	40	40	5.0	A
174	30	40	30	5.0	A
175	40	40	20	5.0	A
176	50	40	10	5.0	A
177	60	40	0	5.0	A
178	0	50	50	5.0	A
179	10	50	40	5.0	A
180	20	50	30	5.0	A
181	30	50	20	5.0	A
182	40	50	10	5.0	A
183	50	50	0	5.0	A
184	0	60	40	5.0	A
185	10	60	30	5.0	A
186	20	60	20	5.0	A
187	30	60	10	5.0	A
188	40	60	0	5.0	A

ID (–)	MXene (wt.%)	CNF (wt.%)	Gelatin (wt.%)	Mixture Loading (mg mL^{-1})	Grade (A/B/C)
189	0	70	30	5.0	A
190	10	70	20	5.0	A
191	20	70	10	5.0	A
192	30	70	0	5.0	A
193	0	80	20	5.0	A
194	10	80	10	5.0	A
195	20	80	0	5.0	A
196	0	90	10	5.0	A
197	10	90	0	5.0	A
198	0	100	0	5.0	A
199	0	0	100	2.5	A
200	10	0	90	2.5	A
201	20	0	80	2.5	B
202	30	0	70	2.5	C
203	40	0	60	2.5	B
204	50	0	50	2.5	B
205	60	0	40	2.5	C
206	70	0	30	2.5	B
207	80	0	20	2.5	B
208	90	0	10	2.5	A
209	100	0	0	2.5	A
210	0	10	90	2.5	B
211	10	10	80	2.5	B
212	20	10	70	2.5	C
213	30	10	60	2.5	C
214	40	10	50	2.5	C
215	50	10	40	2.5	C
216	60	10	30	2.5	C
217	70	10	20	2.5	B
218	80	10	10	2.5	B
219	90	10	0	2.5	A
220	0	20	80	2.5	A
221	10	20	70	2.5	A
222	20	20	60	2.5	B
223	30	20	50	2.5	B
224	40	20	40	2.5	B
225	50	20	30	2.5	B
226	60	20	20	2.5	A
227	70	20	10	2.5	A

ID (–)	MXene (wt.%)	CNF (wt.%)	Gelatin (wt.%)	Mixture Loading (mg mL^{-1})	Grade (A/B/C)
228	80	20	0	2.5	A
229	0	30	70	2.5	A
230	10	30	60	2.5	A
231	20	30	50	2.5	A
232	30	30	40	2.5	A
233	40	30	30	2.5	A
234	50	30	20	2.5	A
235	60	30	10	2.5	A
236	70	30	0	2.5	A
237	0	40	60	2.5	A
238	10	40	50	2.5	B
239	20	40	40	2.5	A
240	30	40	30	2.5	A
241	40	40	20	2.5	A
242	50	40	10	2.5	A
243	60	40	0	2.5	A
244	0	50	50	2.5	A
245	10	50	40	2.5	B
246	20	50	30	2.5	A
247	30	50	20	2.5	A
248	40	50	10	2.5	A
249	50	50	0	2.5	A
250	0	60	40	2.5	A
251	10	60	30	2.5	A
252	20	60	20	2.5	A
253	30	60	10	2.5	A
254	40	60	0	2.5	A
255	0	70	30	2.5	A
256	10	70	20	2.5	A
257	20	70	10	2.5	A
258	30	70	0	2.5	A
259	0	80	20	2.5	A
260	10	80	10	2.5	A
261	20	80	0	2.5	A
262	0	90	10	2.5	A
263	10	90	0	2.5	A
264	0	100	0	2.5	A

Table S2. Testing data points for the SVM classifier.

ID (–)	MXene (wt.%)	CNF (wt.%)	Gelatin (wt.%)	Mixture Loading (mg mL^{-1})	Grade (A/B/C)
1	49	11	40	10.0	A
2	24	42	34	10.0	C
3	65	12	23	10.0	A
4	20	16	64	10.0	A
5	38	33	29	10.0	C
6	30	49	21	10.0	B
7	55	35	10	10.0	A
8	18	62	21	10.0	C
9	31	25	45	10.0	C
10	10	47	43	10.0	B
11	49	11	40	7.5	B
12	24	42	34	7.5	A
13	65	12	23	7.5	A
14	20	16	64	7.5	A
15	38	33	29	7.5	A
16	30	49	21	7.5	A
17	55	35	10	7.5	A
18	18	62	21	7.5	A
19	31	25	45	7.5	A
20	10	47	43	7.5	A
21	49	11	40	5.0	B
22	24	42	34	5.0	A
23	65	12	23	5.0	B
24	20	16	64	5.0	A
25	38	33	29	5.0	A
26	30	49	21	5.0	A
27	55	35	10	5.0	A
28	18	62	21	5.0	A
29	31	25	45	5.0	A
30	10	47	43	5.0	A
31	49	11	40	2.5	B
32	24	42	34	2.5	A
33	65	12	23	2.5	B
34	20	16	64	2.5	A
35	38	33	29	2.5	A
36	30	49	21	2.5	A
37	55	35	10	2.5	A
38	18	62	21	2.5	A

ID (–)	MXene (wt.%)	CNF (wt.%)	Gelatin (wt.%)	Mixture Loading (mg mL^{-1})	Grade (A/B/C)
39	31	25	45	2.5	B
40	10	47	43	2.5	A

Table S3. Training data points for the prediction model.

Loop # (–)	ID (–)	MXene (wt.%)	CNF (wt.%)	Gelatin (wt.%)	GA (+/–)	Mixture Loading (mg mL^{-1})	σ_{30} (kPa)	R_0 (Ω)
1	1	12.4	40.1	47.4	–	10.0	7.8	1.0×10^{10}
1	2	13.1	27.0	59.9	–	10.0	8.9	1.0×10^{10}
1	3	33.3	35.6	31.1	–	10.0	7.3	1.5×10^{2}
1	4	11.2	76.5	12.3	–	10.0	10.3	1.0×0^{10}
1	5	71.0	11.5	17.4	–	10.0	7.1	3.6×10^{0}
1	6	60.6	27.7	11.7	–	10.0	10.5	3.0×10^{0}
1	7	33.3	54.1	12.7	–	10.0	12.1	1.0×10^{2}
1	8	46.9	16.2	36.9	–	10.0	9.4	4.9×10^{0}
1	9	20.2	67.9	11.9	–	10.0	13.8	4.8×10^{2}
1	10	12.4	40.1	47.4	–	7.5	3.3	1.0×10^{10}
1	11	13.1	27.0	59.9	–	7.5	3.2	1.0×10^{10}
1	12	33.3	35.6	31.1	–	7.5	2.0	1.1×10^{4}
1	13	11.2	76.5	12.3	–	7.5	2.9	3.0×10^{7}
1	14	71.0	11.5	17.4	–	7.5	4.7	8.2×10^{0}
1	15	33.3	54.1	12.7	–	7.5	4.1	1.6×10^{4}
1	16	20.2	67.9	11.9	–	7.5	7.8	1.0×10^{4}
1	17	12.4	40.1	47.4	–	5.0	0.7	1.0×10^{10}
1	18	13.1	27.0	59.9	–	5.0	0.7	1.0×10^{10}
1	19	11.2	76.5	12.3	–	5.0	1.0	2.2×10^{7}
1	20	60.6	27.7	11.7	–	5.0	0.6	9.3×10^{2}
1	21	33.3	54.1	12.7	–	5.0	1.3	2.8×10^{1}
1	22	20.2	67.9	11.9	–	5.0	1.9	5.5×10^{3}
2	23	11.2	76.5	12.3	–	2.5	0.2	1.8×10^{7}
2	24	60.6	27.7	11.7	–	2.5	0.3	7.5×10^{1}
2	25	33.3	54.1	12.7	–	2.5	0.2	9.3×10^{2}
2	26	20.2	67.9	11.9	–	2.5	0.1	1.0×10^{6}
2	27	60.6	27.7	11.7	–	7.5	5.0	2.6×10^{1}
2	28	33.3	54.1	12.7	–	7.5	4.6	n/a
2	29	20.2	67.9	11.9	–	7.5	4.5	n/a
2	30	30.4	31.9	37.7	+	10.0	7.9	1.1×10^{2}
2	31	61.5	25.9	12.6	+	10.0	12.7	4.0×10^{3}
2	32	23.0	64.7	12.3	+	10.0	16.1	4.3×10^{2}
2	33	27.5	32.2	40.3	+	7.5	5.0	1.5×10^{2}
2	34	26.8	62.3	10.9	+	7.5	7.1	9.4×10^{1}
2	35	68.4	21.3	10.4	+	7.5	7.1	4.9×10^{1}

Loop # (–)	ID (–)	MXene (wt.%)	CNF (wt.%)	Gelatin (wt.%)	GA (+/–)	Mixture Loading (mg mL^{-1})	σ_{30} (kPa)	R_0 (Ω)
2	36	64.1	15.4	20.5	–	10.0	8.5	1.4×10^0
2	37	10.9	18.9	70.2	–	10.0	3.3	1.0×10^{10}
2	38	9.0	31.4	59.6	–	10.0	8.8	1.0×10^{10}
2	39	24.8	54.1	21.1	–	10.0	10.2	3.1×10^5
2	40	9.9	67.7	22.3	–	10.0	9.9	1.0×10^{10}
2	41	77.0	9.7	13.3	+	10.0	6.2	1.7×10^0
2	42	51.7	25.8	22.5	+	10.0	6.4	5.0×10^0
3	43	21.9	28.9	49.3	+	10.0	6.4	1.0×10^{10}
3	44	37.1	41.6	21.3	+	10.0	5.6	4.6×10^{10}
3	45	77.6	13.1	9.3	–	7.5	3.7	1.7×10^0
3	46	21.5	25.6	53.0	–	7.5	1.7	5.1×10^7
3	47	47.8	33.2	19.0	–	7.5	4.4	2.2×10^1
3	48	27.4	39.6	33.0	+	7.5	4.1	6.3×10^6
3	49	19.2	45.6	35.2	+	7.5	3.8	n/a
3	50	13.0	46.0	41.0	+	7.5	4.1	1.0×10^{10}
3	51	12.0	54.1	34.0	+	7.5	4.6	1.0×10^{10}
3	52	15.3	19.3	65.4	–	5.0	0.3	1.0×10^{10}
3	53	38.7	48.9	12.4	–	5.0	1.5	1.2×10^2
3	54	13.3	50.6	36.1	–	5.0	1.1	1.0×10^{10}
3	55	74.4	17.5	8.1	+	5.0	2.3	n/a
3	56	47.5	32.9	19.6	+	5.0	1.8	3.1×10^1
3	57	28.2	62.9	8.9	+	5.0	1.8	9.5×10^2
3	58	69.9	17.9	12.2	–	2.5	0.2	7.1×10^1
3	59	40.9	38.0	21.1	–	2.5	0.9	5.5×10^4
3	60	31.1	41.0	27.9	–	2.5	0.6	1.0×10^{10}
3	61	30.3	23.9	45.8	–	10.0	12.9	7.3×10^6
3	62	17.6	37.2	45.3	–	10.0	11.2	1.0×10^{10}
4	63	29.7	58.5	11.8	–	10.0	13.1	7.1×10^2
4	64	13.3	62.4	24.4	–	10.0	12.0	1.0×10^{10}
4	65	23.3	48.0	28.7	+	10.0	12.9	3.1×10^6
4	66	18.9	55.1	25.9	+	10.0	13.0	3.9×10^5
4	67	60.6	22.3	17.2	–	7.5	5.5	1.0×10^1
4	68	46.1	41.3	12.6	–	7.5	6.1	4.8×10^1
4	69	17.4	63.2	19.4	–	7.5	5.5	2.3×10^6
4	70	36.6	25.2	38.2	+	7.5	4.1	1.6×10^3
4	71	8.5	31.1	60.4	+	7.5	2.9	1.0×10^{10}

Loop # (–)	ID (–)	MXene (wt.%)	CNF (wt.%)	Gelatin (wt.%)	GA (+/–)	Mixture Loading (mg mL^{-1})	σ_{30} (kPa)	R_0 (Ω)
4	72	40.1	35.7	24.3	+	7.5	5.2	3.5×10^2
4	73	20.9	40.1	39.1	+	7.5	5.9	1.9×10^6
4	74	8.8	33.8	57.4	–	5.0	1.1	1.0×10^{10}
4	75	25.8	48.5	25.7	–	5.0	1.5	2.7×10^6
4	76	12.4	60.3	27.2	–	5.0	1.7	1.0×10^{10}
4	77	18.6	26.9	54.5	+	5.0	1.0	1.0×10^{10}
4	78	25.3	32.3	42.4	+	5.0	1.1	3.5×10^7
4	79	21.7	37.0	41.2	+	5.0	1.2	1.0×10^{10}
4	80	20.6	55.3	24.1	+	5.0	1.6	1.0×10^{10}
4	81	26.0	58.5	15.6	–	2.5	0.2	5.5×10^6
4	82	41.9	47.4	10.7	+	2.5	0.4	1.0×10^{10}
5	83	17.6	72.7	9.7	+	2.5	0.4	1.0×10^{10}
5	84	47.0	28.0	25.1	–	10.0	7.2	2.6×10^1
5	85	52.5	31.4	16.2	–	10.0	7.4	6.4×10^0
5	86	57.6	31.9	10.5	–	10.0	9.6	8.8×10^0
5	87	8.5	47.8	43.7	–	10.0	13.7	1.0×10^{10}
5	88	52.9	18.5	28.7	+	10.0	6.6	1.2×10^2
5	89	22.6	19.4	58.0	+	10.0	8.2	1.0×10^{10}
5	90	26.2	37.0	36.8	+	10.0	14.2	1.3×10^7
5	91	42.2	45.3	12.5	+	10.0	12.8	1.5×10^2
5	92	64.6	11.7	23.7	–	7.5	1.7	2.8×10^3
5	93	15.4	31.9	52.8	–	7.5	3.3	1.0×10^{10}
5	94	53.7	38.5	7.9	–	7.5	4.2	1.2×10^1
5	95	28.8	45.8	25.4	–	7.5	7.3	1.0×10^5
5	96	17.9	55.4	26.7	–	7.5	8.9	1.0×10^{10}
5	97	52.1	27.8	20.1	+	7.5	4.4	6.2×10^1
5	98	20.4	34.6	45.0	+	7.5	5.5	1.0×10^{10}
5	99	39.5	49.3	11.2	+	7.5	5.9	3.1×10^2
5	100	53.3	34.5	12.2	–	5.0	1.3	3.6×10^1
5	101	22.9	42.7	34.4	–	5.0	1.3	1.0×10^{10}
5	102	9.2	82.1	8.7	–	5.0	2.2	1.0×10^{10}
6	103	41.4	34.9	23.7	+	5.0	1.9	1.4×10^4
6	104	16.3	45.1	38.6	+	5.0	1.7	1.0×10^{10}
6	105	8.4	48.1	43.5	+	5.0	1.6	n/a
6	106	43.1	42.0	14.9	–	10.0	7.3	3.7×10^1
6	107	32.0	45.6	22.5	–	10.0	8.7	1.9×10^4

Loop # (–)	ID (–)	MXene (wt.%)	CNF (wt.%)	Gelatin (wt.%)	GA (+/–)	Mixture Loading (mg mL^{-1})	σ_{30} (kPa)	R_0 (Ω)
6	108	36.7	48.6	14.7	–	10.0	9.3	1.0×10^2
6	109	34.0	50.9	15.1	–	10.0	6.2	1.3×10^4
6	110	37.5	51.6	10.9	–	10.0	7.0	1.0×10^3
6	111	23.4	52.5	24.0	+	10.0	9.9	1.5×10^6
6	112	17.8	23.5	58.7	–	7.5	1.2	1.0×10^{10}
6	113	34.9	41.8	23.3	–	7.5	4.0	1.4×10^4
6	114	10.0	45.2	44.7	–	7.5	5.1	1.0×10^{10}
6	115	24.4	60.2	15.4	–	7.5	5.7	1.1×10^5
6	116	30.3	38.3	31.4	+	7.5	8.1	3.7×10^2
6	117	15.0	75.0	9.9	+	7.5	5.6	2.0×10^5
6	118	20.5	31.8	47.7	–	5.0	1.2	1.0×10^{10}
6	119	43.4	32.1	24.5	–	5.0	1.5	2.0×10^3
6	120	19.5	51.8	28.8	–	5.0	2.2	1.0×10^{10}
6	121	45.3	30.7	24.0	+	5.0	1.4	n/a
6	122	18.5	39.0	42.6	+	5.0	2.3	1.0×10^{10}
7	123	9.8	62.2	28.0	+	5.0	3.1	1.0×10^{10}
7	124	38.1	48.2	13.7	–	2.5	0.9	4.4×10^4
7	125	20.5	62.6	16.9	+	2.5	0.6	1.0×10^7
7	126	30.0	38.0	32.0	+	10.0	9.1	n/a
7	127	15.0	55.0	30.0	+	10.0	4.1	n/a
7	128	17.0	40.0	43.0	–	10.0	7.5	n/a
7	129	32.0	50.0	18.0	–	10.0	6.3	n/a
7	130	30.0	32.0	38.0	+	7.5	3.6	n/a
7	131	18.0	47.0	35.0	+	7.5	4.2	n/a
7	132	19.0	35.0	46.0	–	7.5	3.2	n/a
7	133	32.0	42.0	26.0	–	7.5	3.2	n/a
7	134	7.0	58.0	35.0	–	2.5	0.3	n/a
7	135	6.9	27.6	65.6	+	10.0	4.6	n/a
7	136	81.1	16.5	2.4	+	10.0	11.0	n/a
7	137	73.8	11.7	14.5	+	10.0	6.4	n/a
7	138	23.9	23.9	52.2	+	10.0	3.7	n/a
7	139	12.5	47.4	40.1	+	10.0	7.4	n/a
7	140	20.8	38.5	40.7	+	10.0	5.6	n/a
7	141	2.4	23.3	74.4	–	10.0	3.1	n/a
7	142	23.0	38.1	38.9	–	10.0	6.9	n/a
8	143	2.8	81.2	16.0	–	7.5	3.2	n/a
8	144	43.5	51.6	4.8	–	7.5	3.6	n/a

Loop # (–)	ID (–)	MXene (wt.%)	CNF (wt.%)	Gelatin (wt.%)	GA (+/–)	Mixture Loading (mg mL^{-1})	σ_{30} (kPa)	R_0 (Ω)
8	145	26.5	42.7	30.8	–	7.5	2.3	n/a
8	146	60.7	31.4	7.9	–	7.5	2.8	n/a
8	147	23.8	70.3	5.9	+	7.5	3.7	n/a
8	148	76.2	5.7	18.1	+	7.5	1.0	n/a
8	149	19.0	25.4	55.6	+	7.5	1.4	n/a
8	150	25.8	53.6	20.6	+	7.5	2.9	n/a
8	151	1.2	25.2	73.6	–	5.0	0.4	n/a
8	152	18.0	33.2	48.8	+	5.0	1.6	n/a
8	153	20.1	30.3	49.6	+	5.0	2.8	n/a
8	154	35.5	41.4	23.1	–	5.0	0.5	n/a
8	155	53.5	44.9	1.6	+	5.0	2.3	n/a
8	156	42.8	52.2	5.0	+	2.5	2.2	n/a
8	157	10.4	18.1	71.5	–	2.5	0.1	n/a
8	158	90.3	1.5	8.3	–	2.5	0.0	n/a
8	159	22.3	53.9	23.8	–	2.5	0.3	n/a
8	160	36.6	39.6	23.8	–	2.5	0.1	n/a
8	161	66.7	22.7	10.6	+	2.5	0.2	n/a
8	162	64.7	29.5	5.9	+	2.5	0.4	n/a

Table S4. Testing data points for the prediction model.

ID (–)	MXene (wt.%)	CNF (wt.%)	Gelatin (wt.%)	GA (+/–)	Mixture Loading (mg mL^{-1})	σ_{30} (kPa)	R_0 (Ω)
1	69.5	23.6	6.9	+	10.0	5.9	n/a
2	37.1	17.4	45.5	–	10.0	2.7	1.2×10^{3}
3	73.4	12.4	14.2	–	10.0	5.5	1.6×10^{1}
4	19.2	24.2	56.6	+	10.0	2.8	1.0×10^{10}
5	7.3	64.8	27.9	+	10.0	3.9	1.1×10^{7}
6	31.4	53.0	15.6	+	10.0	8.2	n/a
7	23.0	35.5	41.6	–	7.5	3.5	1.0×10^{10}
8	36.3	56.0	7.6	–	7.5	3.7	n/a
9	88.8	5.1	6.1	+	7.5	1.8	2.7×10^{1}
10	34.3	61.2	4.5	+	7.5	2.9	1.1×10^{3}
11	73.2	20.0	6.8	+	5.0	1.3	5.1×10^{1}
12	31.8	60.1	8.1	–	5.0	1.1	1.9×10^{4}
13	10.9	84.2	4.8	–	5.0	3.2	n/a
14	35.2	42.0	22.8	+	5.0	0.7	6.9×10^{3}
15	17.5	28.8	53.7	–	5.0	1.9	1.0×10^{10}
16	4.7	52.0	43.2	+	5.0	2.3	1.0×10^{10}
17	59.8	26.0	14.2	–	2.5	0.2	1.1×10^{3}

Table S5. Comparison between experimental and model-predicted σ_{30} and R_0 values in Fig. 3a.

Recipe Number	MXene (wt.%)	CNF (wt.%)	Gelatin (wt.%)	GA (+/–)	Mixture Loading (mg mL^{-1})	Experimental		Model-Predicted	
						σ_{30} (kPa)	R_0 (Ω)	σ_{30} (kPa)	R_0 (Ω)
1	36.7	48.6	14.7	–	10.0	9.3	1.0×10^{2}	8.9	1.1×10^{2}
2	46.1	41.3	12.6	–	7.5	6.1	4.8×10^{1}	6.0	4.9×10^{1}
3	12.4	40.1	47.4	–	5.0	0.7	1.0×10^{10}	0.9	1.1×10^{10}
4	31.1	41.0	27.9	–	2.5	0.6	1.0×10^{10}	0.4	1.0×10^{10}
5	42.2	45.3	12.5	+	10.0	12.8	1.5×10^{2}	12.6	1.6×10^{2}
6	68.4	21.3	10.4	+	7.5	7.1	5.0×10^{0}	7.0	4.6×10^{0}
7	47.5	32.9	19.6	+	5.0	1.8	3.1×10^{1}	1.9	3.2×10^{1}
8	20.5	62.6	16.9	+	2.5	0.6	$1. \times 10^{7}$	0.6	1.0×10^{7}

Table S6. Property requirements, model-suggested fabrication parameters, and experimental results in Fig. 3c.

Property Requirement		Model-Suggested Fabrication Parameters						Experimental Results	
Mechanical Property	Electrical Property	Recipe Number	MXene (wt.%)	CNF (wt.%)	Gelatin (wt.%)	GA (+/–)	Mixture Loading (mg mL^{-1})	σ_{30} (kPa)	R_0 (Ω)
$\sigma_{30} > 10.0$ kPa	–	9	22.0	66.0	12.0	+	10.0	13.8 ± 0.7	n/a
		10	58.0	32.0	10.0	+	10.0	12.2 ± 0.3	n/a
$\sigma_{30} > 10.0$ kPa	$R_0 < 10.0\ \Omega$	11	64.0	24.0	12.0	+	10.0	12.6 ± 0.4	8.9 ± 1.8
		12	66.0	24.0	10.0	+	10.0	13.9 ± 1.2	7.2 ± 0.6
		13	62.0	26.0	12.0	+	10.0	12.1 ± 1.0	10.1 ± 1.0
		14	72.0	22.0	6.0	+	10.0	14.9 ± 0.6	5.4 ± 0.2

Table S7. Comparison of our AI/ML integrated approach for conductive aerogels with the state-of-the-art works.

Aerogel Design Strategy	Aerogel Composition	Aerogel Density (mg cm^{-3})	σ_{30} (kPa)	Electrical Property	Electrical Property Measurement	Ref.
AI/ML framework	MXene/CNF/gelatin/GA	2.0 – 14.0	0.05 – 16.1	1.4 – 10^{10} Ω	Two-electrode testing system	This work
Design of experiment	rGO	2.3	6.0	1.6×10^{1} S cm^{-1}	Four-point probe	3
Design of experiment	MXene/CNF	4.0	0.5	2.8×10^{1} S cm^{-1}	Four-point probe	4
Design of experiment	MXene/CNF	4.0	0.8	4.0×10^{-1} S cm^{-1}	Four-point probe	4
Design of experiment	MTMS treated bacterial cellulose/MXene	6.2	1.6	1.2×10^{2} S cm^{-1}	Four-point probe	5
Design of experiment	CNF/MXene/CNT	7.5	0.4	2.4×10^{3} S cm^{-1}	Four-point probe	6
Design of experiment	rGO	8.5	8.2	4.3×10^{1} S cm^{-1}	Four-electrode testing system	7
Design of experiment	MXene/CNT	9.1	0.5	4.5×10^{2} S cm^{-1}	Four-point probe	8
Design of experiment	PGPDMS/MXene	9.9	0.1	–	–	9
Design of experiment	GO/PVA	10.0	5.0	3.0×10^{0} S cm^{-1}	Source meter	10
Design of experiment	MXene/rGO	12.2	7.5	3.6×10^{1} S cm^{-1}	Three-electrode setup	11
Design of experiment	MXene	12.6	1.0	5.4×10^{1} S cm^{-1}	Two-electrode testing system	12
Design of experiment	MXene/CNF/PMDI	18.0	40.0	1.1×10^{0} Ω cm	Four-point probe	13
Design of experiment	GO	25.0	1.0	9.7×10^{0} S cm^{-1}	Source meter	14

Aerogel Design Strategy	Aerogel Composition	Aerogel Density (mg cm^{-3})	σ_{30} (kPa)	Electrical Property	Electrical Property Measurement	Ref.
Design of experiment	MXene/ANF	25.0	17.0	1.0×10^4 Ω cm	Two-electrode testing system	15
Design of experiment	MXene/CNT/ANF	42.0	2.3	2.7×10^0 Ω cm	Four-point probe	16
Design of experiment	MXene/CNT/ANF	42.0	0.8	2.0×10^{-1} Ω cm	Four-point probe	16
Design of experiment	CNF/MXene	50.0	7.0	2.6×10^1 Ω cm	Two-electrode testing system	17
Design of experiment	CNF/MXene	50.0	3.4	1.4×10^1 Ω cm	Two-electrode testing system	17
Design of experiment	MXene/WPU	–	3.0	–	–	18

Abbreviations

rGO: Reduced graphene oxide

GO: Graphene oxide

MTMS: Methyltrimethoxysilane

CNT: Carbon nanotube

PGPDMS: Glycidoxypropyldimethoxymethylsilane

PVA: Poly(vinyl alcohol)

PMDI: Poly((phenyl isocyanate)-co-formaldehyde)

ANF: Aramid nanofiber

WPU: Waterborne polyurethane

Table S8. Structural features of conductive aerogels extracted from the SEM images in Fig. 4c.

FE Model Name	Mixture Loading (mg mL^{-1})	Average Pore Width (µm)	Average Pore Height (µm)	Wall Thickness (µm)	Tuning Parameter (β_{imp})	Young's Modulus (MPa)	Poisson's Ratio (ν)	Pore Density (ρ)	Pore Aspect Ratio (ψ)
High-Density	10.0	18.2	6.4	0.3	0.3	3,440.7	0.5	5.4×10^{-2}	2.8
Medium-Density	7.5	28.3	17.8	0.3	0.3	3,440.7	0.5	2.9×10^{-2}	1.6
Low-Density	5.0	39.1	19.0	0.3	0.3	3,440.7	0.5	2.5×10^{-2}	2.1

Table S9. Compositions and mixture loadings of model-suggested conductive aerogels in Fig 5b.

Recipe Number	MXene (wt.%)	CNF (wt.%)	Gelatin (wt.%)	GA (+/–)	Mixture Loading (mg mL^{-1})	σ_{30} (kPa)	R_0 (Ω)
15	64.1	15.4	20.5	–	10.0	8.5	1.4
16	77.6	13.1	9.3	–	7.5	4.0	1.7
17	60.6	27.7	11.7	–	7.5	5.3	2.7
18	71.0	11.5	17.4	–	10.0	7.1	3.6
19	51.6	38.4	10.0	–	10.0	7.6	4.1
20	68.4	21.3	10.4	+	7.5	7.1	4.9
21	51.7	25.8	22.5	+	10.0	6.4	5.0
22	71.0	11.5	17.4	–	7.5	4.7	8.2
23	60.6	22.3	17.2	–	7.5	5.5	10.3
24	53.7	38.5	7.9	–	7.5	4.2	12.4
25	47.8	33.2	19.0	–	7.5	4.4	21.7

Movie S1. Automatic pipetting robot (i.e., OT-2 robot) capable of preparing mixed dispersions with various MXene/CNF/gelatin/GA ratios and mixture loadings.

Movie S2. UR5e robotic arm capable of automating the compression tests of conductive MXene aerogels.

Supporting References

1 Hung Anh, L. D. & Pásztory, Z. An Overview of Factors Influencing Thermal Conductivity of Building Insulation Materials. *J. Build. Eng.* **44**, 102604 (2021).

2 Overvelde, J. T. B. & Bertoldi, K. Relating Pore Shape to the Non-Linear Response of Periodic Elastomeric Structures. *J. Mech. Phys. Solids* **64**, 351–366 (2014).

3 Moon, I. K., Yoon, S., Chun, K.-Y. & Oh, J. Highly Elastic and Conductive N-Doped Monolithic Graphene Aerogels for Multifunctional Applications. *Adv. Funct. Mater.* **25**, 6976–6984 (2015).

4 Zeng, Z. *et al.* Nanocellulose-MXene Biomimetic Aerogels with Orientation-Tunable Electromagnetic Interference Shielding Performance. *Adv. Sci.* **7**, 2000979 (2020).

5 Zhao, D. *et al.* Multifunctional, Superhydrophobic and Highly Elastic MXene/Bacterial Cellulose Hybrid Aerogels Enabled *via* Silylation. *J. Mater. Chem. A* **10**, 24772–24782 (2022).

6 Xu, T. *et al.* Nanocellulose-Assisted Construction of Multifunctional MXene-Based Aerogels with Engineering Biomimetic Texture for Pressure Sensor and Compressible Electrode. *Nano-Micro Lett.* **15**, 98 (2023).

7 Luo, R. *et al.* Super Durable Graphene Aerogel Inspired by Deep-Sea Glass Sponge Skeleton. *Carbon* **191**, 153–163 (2022).

8 Deng, Z., Tang, P., Wu, X., Zhang, H.-B. & Yu, Z.-Z. Superelastic, Ultralight, and Conductive $Ti_3C_2T_x$ MXene/Acidified Carbon Nanotube Anisotropic Aerogels for Electromagnetic Interference Shielding. *ACS Appl. Mater. Interfaces* **13**, 20539–20547 (2021).

9 Shi, X. *et al.* Pushing Detectability and Sensitivity for Subtle Force to New Limits with Shrinkable Nanochannel Structured Aerogel. *Nat. Commun.* **13**, 1119 (2022).

10 Yang, M. *et al.* Biomimetic Architectured Graphene Aerogel with Exceptional Strength and Resilience. *ACS Nano* **11**, 6817–6824 (2017).

11 Jiang, D. *et al.* Superelastic $Ti_3C_2T_x$ MXene-Based Hybrid Aerogels for Compression-Resilient Devices. *ACS Nano* **15**, 5000–5010 (2021).

12 Tetik, H. *et al.* 3D Printed MXene Aerogels with Truly 3D Macrostructure and Highly Engineered Microstructure for Enhanced Electrical and Electrochemical Performance. *Adv. Mater.* **34**, 2104980 (2022).

13 Wu, N. *et al.* Ultrathin Cellulose Nanofiber Assisted Ambient-Pressure-Dried, Ultralight, Mechanically Robust, Multifunctional MXene Aerogels. *Adv. Mater.* **35**, 2207969 (2023).

14 Pang, K. *et al.* Hydroplastic Foaming of Graphene Aerogels and Artificially Intelligent Tactile Sensors. *Sci. Adv.* **6**, eabd4045 (2020).

15 Wang, L., Zhang, M., Yang, B., Tan, J. & Ding, X. Highly Compressible, Thermally Stable, Light-Weight, and Robust Aramid Nanofibers/Ti_3AlC_2 MXene Composite Aerogel for Sensitive Pressure Sensor. *ACS Nano* **14**, 10633–10647 (2020).

16 Yan, Z. *et al.* MXene/CNTs/Aramid Aerogels for Electromagnetic Interference Shielding and Joule Heating. *ACS Appl. Nano Mater.* **6**, 6141–6150 (2023).

17 Xu, W., Wu, Q., Gwon, J. & Choi, J.-W. Ice-Crystal-Templated “Accordion-Like” Cellulose Nanofiber/MXene Composite Aerogels for Sensitive Wearable Pressure Sensors. *ACS Sustainable Chem. Eng.* **11**, 3208–3218 (2023).

18 Cai, C., Wei, Z., Huang, Y. & Fu, Y. Wood-Inspired Superelastic MXene Aerogels with Superior Photothermal Conversion and Durable Superhydrophobicity for Clean-up of Super-Viscous Crude Oil. *Chem. Eng. J.* **421**, 127772 (2021).